

Virtual Agonist-antagonist Mechanisms Produce Biological Muscle-like Functions: An Application for Robot Joint Control

Xiaofeng Xiong¹, Florentin Wörgötter¹ and Poramate Manoonpong^{1,2}

¹Bernstein Center for Computational Neuroscience, University of Göttingen, Göttingen, Germany

²Maesk Mc-Kinney Moller Institute, University of Southern Denmark, Odense M, Denmark

Abstract

Purpose – Biological muscles of animals have a surprising variety of functions, i.e., struts, springs, and brakes. According to this, the purpose of this paper is to apply virtual agonist-antagonist mechanisms to robot joint control allowing for muscle-like functions and variably compliant joint motions.

Design/methodology/approach – Each joint is driven by a pair of virtual agonist-antagonist mechanism (VAAM, i.e., passive components). The muscle-like functions as well as the variable joint compliance are simply achieved by tuning the damping coefficient of the VAAM.

Findings – With the VAAM, variably compliant joint motions can be produced without mechanically bulky and complex mechanisms or complex force/torque sensing at each joint. Moreover, through tuning the damping coefficient of the VAAM, the functions of the VAAM are comparable to biological muscles.

Originality/value – The model (i.e., VAAM) provides a way forward to emulate muscle-like functions that are comparable to those found in physiological experiments of biological muscles. Based on these muscle-like functions, the robotic joints can easily achieve variable compliance that does not require complex physical components or torque sensing systems; thereby capable of implementing the model on small legged robots driven by, e.g., standard servo motors. Thus, the VAAM minimizes hardware and reduces system complexity. From this point of view, the model opens up another way of simulating muscle behaviors on artificial machines.

Executive summary

The VAAM can be applied to produce variable compliant motions of a high DOF robot. Only relying on force sensing at the end effector, this application is easily achieved by changing coefficients of the VAAM. Therefore, the VAAM can reduce economic cost on mechanical and sensing components of the robot, compared to traditional methods (e.g., artificial muscles).

Keywords Agonist and antagonist muscles, Position control, Hexapod robot

Paper type Research paper

1. Introduction

Muscles are usually considered as motors that produce mechanical work (Nishikawa et al., 2007). In fact, they perform multiple functions like brakes, dampers, and struts (Dickinson et al., 2000). For example, muscles in running cockroaches may act as brakes for absorbing power to maintain stability (Ahn et al., 2002). In turkey level running, they may serve as struts for storing and recovering energy of spring-like tendons (Gabaldon et al., 2004). The multiple muscle functions enable animals to accomplish locomotor stability and mobility over difficult terrains (Full et al., 2002; Fish et al., 2002). In general, muscles are modelled by active and passive components. While the active components basically generate coordinated movements, the passive components play a major role in locomotor stability (Dudek et al., 2006; Haeufle et al., 2010). For example, cockroaches mainly rely on the passive components of their muscles for maintaining stability over highly complex terrain consisting of obstacles up to three times of the cockroach hip height (Sponberg et al., 2008). To our knowledge, there is no computational model that can generate muscle-like functions and be applied to control real robotic joints.

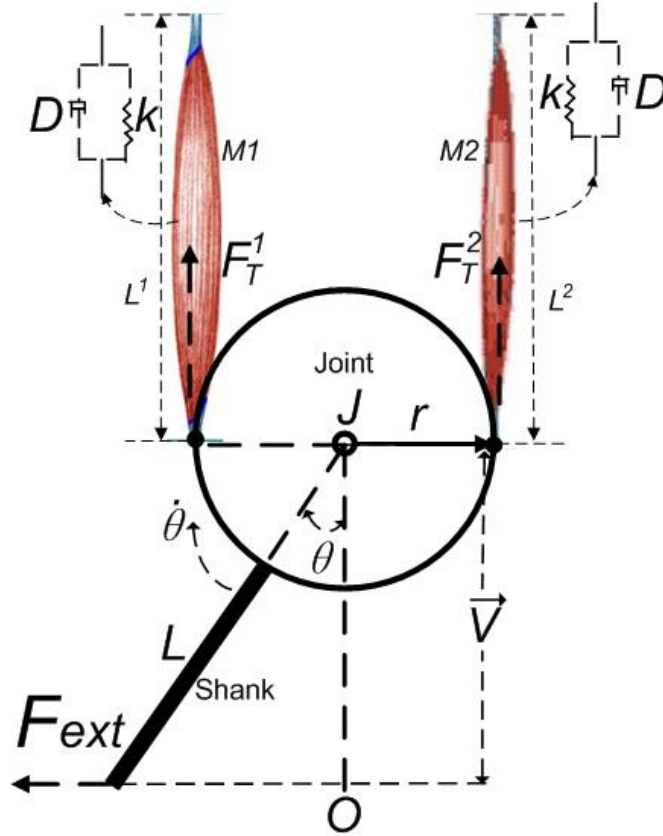
Inspired by the biological principles mentioned above, the aim of this work is to apply virtual agonist-antagonist mechanisms to robot joint control allowing for muscle-like functions and variably compliant joint motions. A pair of virtual agonist-antagonist mechanism (i.e., VAAM) consists of spring-damper components. 'Virtual' here means the joint, which is physically actuated by a standard servo motor, can produce variably compliant motions as if it were driven by a pair of physical agonist-antagonist muscles. The joint controlled by the VAAM can produce variably compliant motions without mechanically complex mechanisms, e.g., variable stiffness actuators (VSAs) (Ham et al., 2009) and artificial muscles (Schmitt et al., 2012). Moreover,

the muscle-like functions of the VAAM shown in this work¹ are comparable to those (i.e., brakes, dampers, and struts) found in physiological experiments of animal muscles (Dickinson *et al.*, 2000).

2. Approach

The pairs of virtual agonist-antagonist mechanism (i.e., VAAM) are proposed for variable compliance control of robotic joints. Specifically, each joint is driven by a pair of the VAAM (i.e., $M1$ and $M2$ in Figure 1). $M1$ and $M2$ are modelled by spring-damper systems, considered as virtual passive elements. They mimic the functions of agonist and antagonist muscles when confronted with an external load (i.e., F_{ext} , see Figure 1). The antagonistic joint (i.e., J) motions are excited by the external load F_{ext} via a shank with the length L . The antagonist mechanism $M2$ resists the extension of the joint angle θ when it is excited by F_{ext} . Simultaneously, the agonist mechanism $M1$ produces an opposing force against $M2$. The directions of F_T^1 and F_{ext} are clockwise when the direction of F_T^2 is counter-clockwise.

Figure 1 Virtual agonist-antagonist mechanism (i.e., VAAM) for antagonistic joint control



Note: The joint J is driven by a pair of the VAAM with lengths L^1 and L^2 (i.e., $M1$ and $M2$). Each of the VAAM consists of a passive element, which is modeled as a spring-damper system. The external force F_{ext} drives the joint J with the radius r via the shank with the length L . θ is the angle of the joint J

Based on Euler's laws, the control equation of antagonistic joint (i.e., the joint J in Figure 1) motions is given by:

$$\ddot{\theta} I = F_{ext} \vec{V} - 2r^2(\theta K + \dot{\theta} D), \vec{V} = (L + r) \cos \theta, \quad (1)$$

where I is the moment of inertia. \vec{V} is the displacement vector of F_{ext} relative to the joint J . r is the radius of the joint J . K and D are stiffness and damping coefficients. The details of Eq. (1) can be seen at Eq. (13) of (Xiong *et al.*, 2013). Note that the VAAM can be applied to joint compliance control in any force dimension if external force F_{ext} that influences joint motion can be sensed. However, here we consider on vertical force since our hexapod robot used for experiments here can detect only vertical force. In the future, we will implement additional sensors that can detect force in other directions.

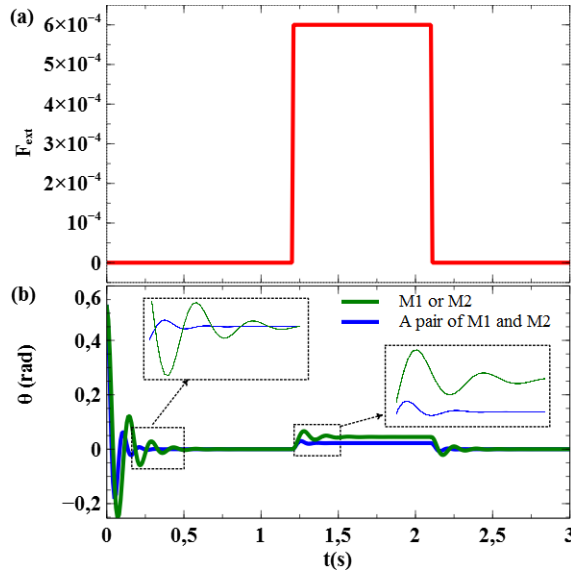
Changing damping coefficients D of $M1$ and $M2$ enables the joint to easily achieve variably compliant motions against an external perturbation when keeping stiffness coefficients K constant. This achievement differs from that of physical antagonistic

¹ This work is an updated and revised version of the work originally presented at the 16th International Conference on Climbing and Walking Robots and the Support Technologies for Mobile Machines (CLAWAR, 2013), Sydney, Australia, 14-17 July 2013.

actuators where two actuators controlled by nonlinear springs are coupled antagonistically, working against each other (Ham *et al.*, 2009; Vanderborcht *et al.*, 2013). These antagonistic actuators (e.g., variable impedance actuators) are still too bulky and energy inefficient to be applied to small legged robots (less than 8 kg). In contrast the VAAM simulates a muscle pair (i.e., $M1$ and $M2$) which is applied here to control only one motor. By doing so, the VAAM generates more power driving the motor to achieve fast joint stability when receiving a certain load (see Figure 2). Moreover, the muscle-like functions of $M1$ and $M2$ are comparable to those of biological muscles (see Section 3).

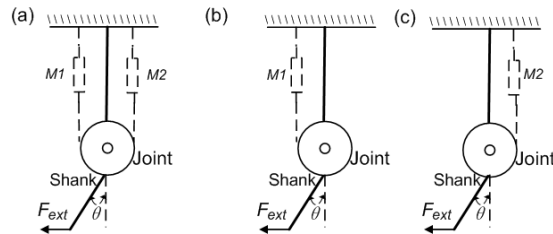
One of the reasons why an agonist-antagonist setup is required is the fact that a pair of the muscles acting in concert can generate more power than the sum of them acting individually when receiving a certain load (Farahat *et al.*, 2010). Besides, a pair of the VAAM allows for faster joint stability (see Figure 2), compared to a single agonist or antagonist mechanism (see Figures 3 (b) and (c)). One can see that the joint driven by $M1$ or $M2$ leads to slower joint stability than when it is driven by a pair of $M1$ and $M2$. Thus, a pair of $M1$ and $M2$ outperforms the other configurations by fast stabilizing joint movement.

Figure 2 Stability comparisons



Notes: (a) Exciting force F_{ext} . (b) Joint angle θ . Green line: $M1$ or $M2$; blue line: a pair of $M1$ and $M2$. All $M1$ and $M2$ have the same stiffness and damping coefficients K and D , i.e., $K = 10$, $D = 0.1$. The joint driven by $M1$ or $M2$ shows more vibrations. In contrast, the joint driven by a pair of $M1$ and $M2$ reaches faster joint stability than when it is driven by only $M1$ or $M2$

Figure 3 Comparisons of different configurations of $M1$ and $M2$



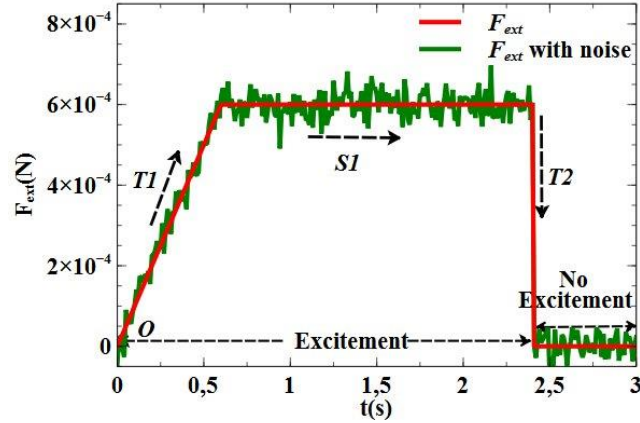
Notes: (a) A pair of $M1$ and $M2$. (b) Only $M1$ (c) Only $M2$

3. Findings

We find that the muscle-like functions (e.g., springs) are achieved by a pair of the VAAM by tuning damping coefficients D of $M1$ and $M2$ (i.e., see Eq. (1)). Typically, the muscle-like functions are characterized by the work loop technique. The technique, prevailing in muscle physiology, can be used to assess the mechanical work and power output of musculoskeletal contractions via in-vitro muscle tests (Biewener, 2003; Ahn, 2012). The roles of muscles (e.g., brakes, dampers, and struts) can be inferred by the shapes of their work loops. Note that the stiffness coefficients K (see Eq. (1)) of $M1$ and $M2$ are kept as constants.

Using F_{ext} and F_{ext} with noise (i.e., error) (see Figure 4), the force-length loops ($F_T^{(1,2)} - L^{(1,2)}$) of $M1$ and $M2$ are shown in Figure 5. They show that $M1$ and $M2$ can perform the muscle-like functions, which are achieved by tuning the damping coefficients D of $M1$ and $M2$.

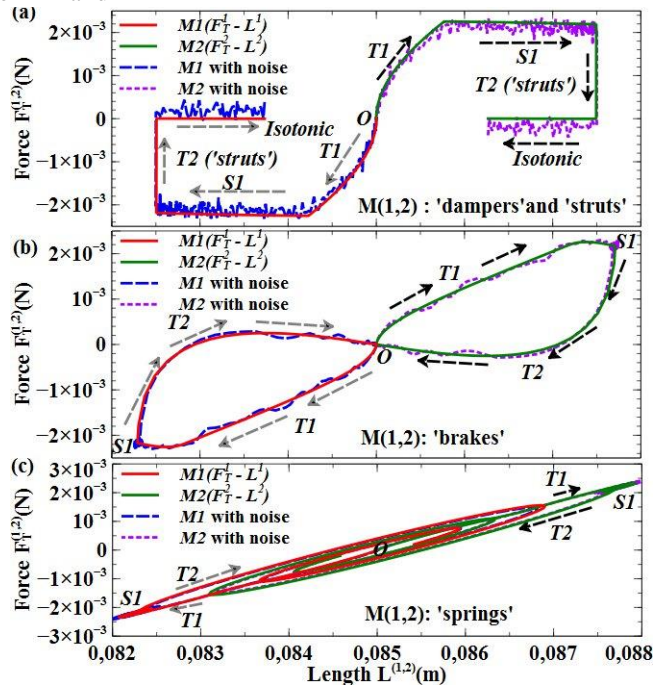
Figure 4 The exciting forces F_{ext} and F_{ext} with noise



Note: After the transition $T1$, F_{ext} is constant (i.e. the state SI). It abruptly goes back to the original position O at the transition $T2$. F_{ext} with noise is the sum of F_{ext} and sampled random noise from a normal (Gaussian) distribution

For instance, the force-length loop ($F_T^2 - L^2$) in Figure 5 (a) shows that $M2$ is lengthening; thereby, it generates force during periods $T1$ and SI . This also results in absorbing mechanical energy. Afterwards it acts as a strut during period $T2$. Finally, it performs an isotonic-like contraction, i.e. shortening without changing force (note that $F_T^2 \neq 0$). Overall, $M2$ (or $M1$) acts as a damper and a strut when their K and D are set as: $K=0.8$, $D = 0.7$. The damper means that muscles only absorb energy. The damper role shown in this paper is comparable to that observed in cockroach running (Full *et al.*, 1998) and guinea fowl running over uneven terrain (Daley *et al.*, 2006). Besides, the strut means that muscles produce force without changing their lengths, i.e. isometric-like contraction. The strut role shown here is comparable to that observed in turkey level running (Gabaldon *et al.*, 2004). Figure 5 (b) presents two clockwise force-length loops. The loops show that $M1$ and $M2$ act as viscoelastic elements for absorbing energy (i.e., brakes) when their K and D are set as: $K = 0.8$, $D = 0.1$. The brake means that muscles perform as viscoelastic elements that absorb energy. The brake role presented in this work is comparable to that found in cockroach experiments (Ahn *et al.*, 2002, Sponberg *et al.*, 2011). Figure 5 (c) shows $M1$ and $M2$ yield slanted straight force-length loops, i.e., $T1$ and $T2$. This means that $M1$ and $M2$ act as springs. The spring role shown here is comparable to that in wing muscles of flies (Tu *et al.*, 1996). On the other hand, different damping coefficients D enable $M1$ and $M2$ to variably react against F_{ext} with noise. One can see that a pair of 'softer' $M1$ and $M2$ (i.e., $D = 0.1$ or 0.01 , see Figures 5 (b) and (c)) acts well against noisy F_{ext} , compared to a 'stiffer' pair (i.e., $D = 0.7$, see Figure 5 (a)). Thus, the permanent error (i.e., noise) of contact force signals will be cancelled due to lower D values of the VAAM (e.g., $D = 0.1$ or 0.01).

Figure 5 Muscle-like functions of $M1$ and $M2$



Notes: Excited by F_{ext} (see Figure 4), these muscle-like functions are achieved via changing damping coefficients D of $M1$ and $M2$. Besides, changing D value leads to different performances of $M1$ and $M2$ against F_{ext} with noise (see Figure 4). (a) $D = 0.7$. $M1$ and $M2$ act as a damper and a strut. (b) $D = 0.1$. $M1$ and $M2$ act as brakes. (c) $D = 0.01$. $M1$ and $M2$ act as springs. Here we set all stiffness coefficients $K = 0.8$. All force-length loops of $M1$ and $M2$ are comparable to those found in physiological experiments of animal muscles (see more details in Figure 3 of (Dickinson *et al.*, 2000))

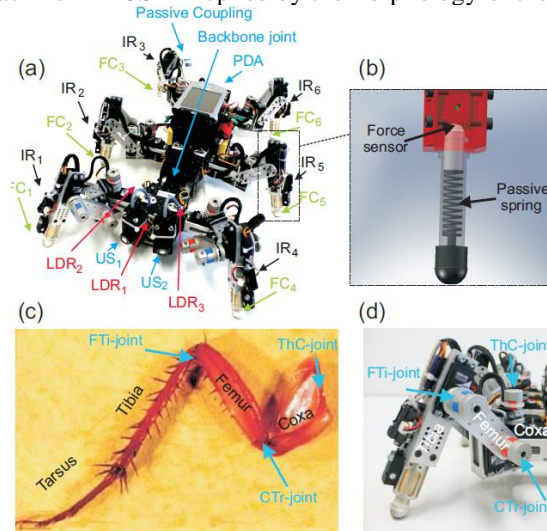
Note that the force-length loops ($F_T^{(1,2)} - L^{(1,2)}$) in Figure 5 (a) cannot return to the original point O like the loops in Figures 5 (b) and (c). This is because $M1$ and $M2$ act as dampers mainly absorbing mechanical energy when their K and D are set as: $K = 0.8$, $D = 0.7$. Figure 5 also shows variable lengthening/shortening ranges of $M1$ and $M2$. The lower the damping coefficients D of $M1$ and $M2$, the larger range they shorten and lengthen. For example, the range of $M1$ is [0.082 (m), 0.085 (m)] and the range of $M2$ is [0.085 (m), 0.088 (m)], when their K and D are set as: $K = 0.8$, $D = 0.01$.

4. Experiments and Results

In the experiments, the VAAM (i.e., $M1$ and $M2$) is implemented on the joints of the hexapod robot AMOS II (see Figure 6). AMOS II is a biologically inspired hardware platform consisting of six identical legs. Each leg has three joints: The thoraco-coxal (ThC-) joint enables forward and backward movements, the coxa-trochanteral (CTr-) joint enables elevation and depression of the leg, and the femur-tibia (FTi-) joint enables extension and flexion of tibia (Figure 6). The morphology of these multi-jointed legs is modelled on the basis of a cockroach leg, but the tarsus segments are ignored (Figure 6 (c)). In addition, a passive coupling is installed at each joint in order to yield compliance and to protect the motor shaft. All leg joints including the backbone joint are driven by digital servomotors. Each leg contains a spring compliant element and a force sensor to measure ground contact force (see Figure 6 (b)). Although the leg has passive physical compliant mechanisms, these mechanisms can only produce certain less compliance to deal with very small disturbances.

The size of AMOS II is 30 (cm) wide, 40 (cm) long, 22 (cm) high. The weight of the fully equipped robot (including 19 servomotors, all electronic components, sensors, and a mobile processor) is approximately 4.5 (kg). The robot has six infrared sensors ($IR_{(1,...,6)}$) at its legs, six force sensors ($FC_{(1,...,6)}$) in its tibiae, three light dependent resistor sensors ($LDR_{(1,2)}$) arranged in a triangle shape on the front body part, and two ultrasonic sensors ($US_{(1,2)}$) at the front body part (see Figure 6). The infrared sensors are used for detecting obstacles near the legs while the ultrasonic sensors are used for detecting obstacles in front. The light dependent resistor sensors serve to generate positive tropism like phototaxis. All these sensors are not used here except the force sensors $FC_{(1,...,6)}$ which are used to detect the exciting force F_{ext} . The force is used to activate the VAAM (i.e., $M1$ and $M2$). We use a Multi-Servo IO-Board (MBoard) installed inside the body to digitize all sensory input signals and to generate a pulse-width-modulated signal to control servomotor position. The MBoard can be connected to a personal digital assistant (PDA) or a personal computer (PC) via an RS232 interface. For the robot experiments, here, the MBoard is connected to a PC on which the control equation of the VAAM is implemented.

Figure 6 The six-legged walking machine AMOS II inspired by the morphology of the American cockroach



Notes: (a) AMOS II and its sensors. (b) Its leg with a force sensor. (c) Cockroach leg (modified from (Zill *et al.*, 2004)). (d) The AMOS II leg with three degrees of freedom

3.1 Reducing Contact Force with a Static Load

$M1$ and $M2$ are applied to the FTi- and CTr-joints of AMOS II (see Figure 7 (a)). The control matrix of $M1$ and $M2$ for the implementation is represented as (derived from Eq. (1)):

$$\ddot{\theta}_{(2 \times 2)} I_{(2 \times 1)} = F_{ext} \vec{V}_{(2 \times 1)} - 2r^2(\theta_{(2 \times 2)} K_{(2 \times 1)} + \dot{\theta}_{(2 \times 2)} D_{(2 \times 1)}), \quad (2)$$

$$\theta_{(2 \times 2)} = \begin{bmatrix} \theta_1 & 0 \\ 0 & \theta_2 \end{bmatrix}, K_{(2 \times 1)} = \begin{bmatrix} K \\ K \end{bmatrix}, D_{(2 \times 1)} = \begin{bmatrix} D \\ D \end{bmatrix}, \quad (3)$$

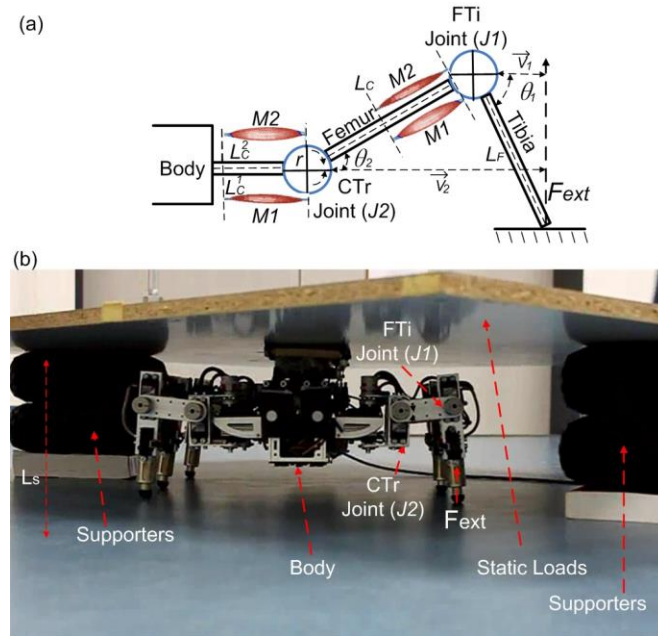
$$I_{(2 \times 1)} = \begin{bmatrix} 5 \times 10^{-7} \\ 5 \times 10^{-7} \end{bmatrix}, \vec{V}_{(2 \times 1)} = \begin{bmatrix} \vec{V}_1 \\ \vec{V}_2 \end{bmatrix}, \quad (4)$$

$$\vec{V}_1 = (L_F + r) \cos \theta_1, \vec{V}_2 = \vec{V}_1 + (L_C + r) \cos \theta_2, \quad (5)$$

where the link lengths L_F and L_C are set as: $L_F = 0.065(\text{m})$, $L_C = 0.11(\text{m})$. r is the joint radius, which is equal to $0.01(\text{m})$. The details of Eqs. (2) and (3) can be seen at Eqs. (16) – (19) of (Xiong *et al.*, 2013).

In this setup (see Figure 7 (b)), AMOS II was placed between supporters having a total height of 18 cm (i.e., $L_s = 18(\text{cm})$). Then we placed a board (i.e., a static load) on top of AMOS II which, thus, carried this load. Thus, the joints of AMOS II have to resist the load when the passive springs fail (i.e., they cannot be compressed anymore). One can see that AMOS II can automatically adapt its height when its legs are driven by $M1$ and $M2$.

Figure 7 Experimental setup

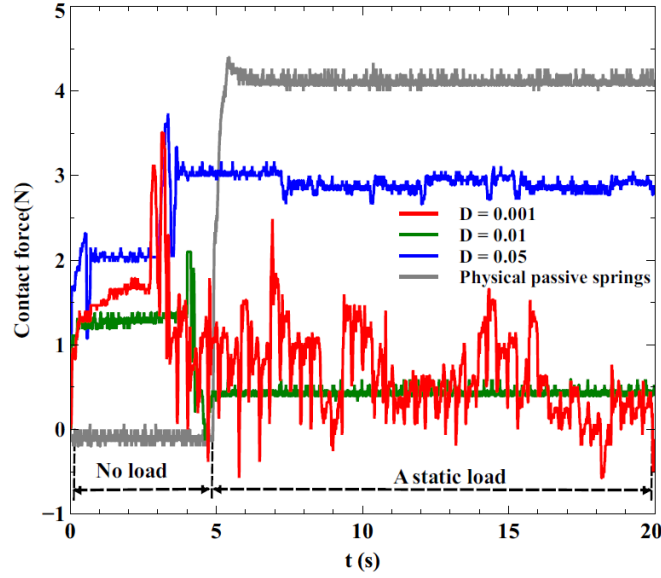


Notes: (a) AMOS II leg where the FTi- and CTr- joints are driven by two pairs of $M1$ and $M2$. The other legs having the same setup are not shown. L_F and L_C are the lengths of the links. L_C^1 and L_C^2 are the lengths of $M1$ and $M2$ that drive the CTr joint. (b) AMOS II experiment with a static load (see texts for details)

In Figure 8, we demonstrate that the legs of AMOS II show less contact force when its joints are driven by $M1$ and $M2$, compared with legs having only passive springs. We empirically adjusted K and D of $M1$ and $M2$. Setting the stiffness and damping coefficients of $M1$ and $M2$ to $K = 0.8$ and $D = 0.01$, this results in less contact force (see $D = 0.01$ in Figure 8). Setting the stiffness and damping coefficients of $M1$ and $M2$ to $K = 0.8$ and $D = 0.01$, this results in less contact force (see $D = 0.01$ in Figure 8). This is because this parameter setup generates proper compliance allowing AMOS II to adapt its body height equally to the height of the supporters (see Figure 7 (b)). Thus, AMOS II and the supporters share the load of the board. These values also make the joints of AMOS II achieve more stable motions (i.e., faster joint stability) compared to the other parameter sets. On the other hand, setting the stiffness and damping coefficients of $M1$ and $M2$ to $K = 0.8$ and $D = 0.05$ results in stiffer legs (i.e., less compliance) pushing the body against the load (see $D = 0.05$ in Figure 8). Setting $K = 0.8$ and $D = 0.001$ leads to springy legs (i.e., unstable joint motions). Thus, this give rise to more bouncing body movement of AMOS II, therefore leading to variation of contact force (see $D = 0.001$ in Figure 8).

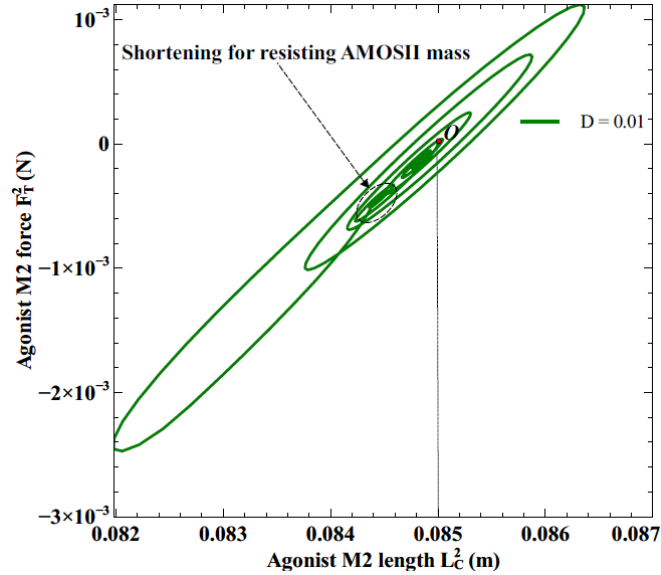
The agonist $M2$ of the CTr- joint shows the similar force-length loop as the agonist $M2$ in Figure 5 (c) when K and D of $M1$ and $M2$ are set as: $K = 0.8$, $D = 0.01$. $M2$ here starts shortening for resisting the mass of AMOS II before receiving the static load. $M2$ initial length is equal to $0.085(\text{m})$ (see O in Figure 9). $M2$ of the CTr- joint here acts as a spring.

Figure 8 Contact forces arise from a static load



Note: Contact forces are recorded from the foot contact force FC_2 . We set the stiffness coefficient K in Eq. (3) to 0.8. After AMOS II is imposed with the static load, the legs with $M1$ and $M2$ show less contact force than without $M1$ and $M2$. Moreover, the legs of AMOS II show stable motion with less contact force when stiffness and damping coefficients of $M1$ and $M2$ are set as: $K = 0.8$ and $D = 0.01$

Figure 9 The force-length loop of $M2$ of the CTr- joint of AMOS II



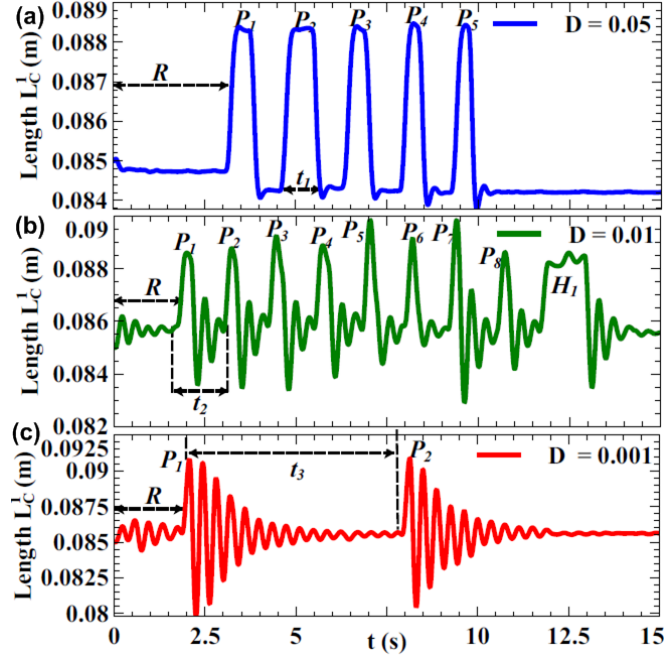
Note: Here the stiffness and damping coefficients K and D of $M2$ are set to: $K = 0.8$, $D = 0.01$. Its force-length loop starts with resisting the mass of AMOS II by shortening (i.e., $M2$ initial length is 0.085(m)). The point O is the starting point of the $M2$ force-length loop

3.2 Variable Joint Stability with Dynamic Loads

The experimental setup of $M1$ and $M2$ of AMOS II here is similar to that shown in Figure 7 (a). However, instead of a static load, dynamic loads were applied here, i.e., hand pushing and holding.

The FTi- and CTr- joints of AMOS II achieve variable stability with different damping coefficients D of Eq. (3). For example, all CTr- joints start resisting the mass of AMOS II by changing the lengths (i.e., L_C^1) of their $M1$ (see "R" region in Figure 10). The CTr- joint stability can be measured by the length L_C^1 , since L_C^1 is proportional to the CTr- joint angle θ_2 .

Figure 10 Joint stability with dynamical loads



Notes: Here we set the stiffness coefficient K in Eq.(3) to 0.8. The dynamical loads are random hand pushing $P_i (i \in [1,8])$ and holding H_1 . Stability of the CTr- joints varies over different damping coefficients D . (a) $D = 0.05$. (b) $D = 0.01$. (c) $D = 0.001$

The CTr- joint motions vary with different damping coefficients D when receiving hand pushing $P_i (i \in [1,8])$ and holding H_1 (see Figure 10 (b)). The CTr- joints achieve faster joint stability when their stiffness and damping coefficients K and D are set to $K = 0.8, D = 0.05$ (see the time of the CTr-joint stability: $t_1 < t_2 < t_3$). In addition, variable 'stiff'/soft' interactions can also be achieved by tuning the damping coefficients D . These diverse interactions include unexpected hand pushing, heavy imposed loads, and vertical AMOS II dropping. 'Soft' here means joints do not resist against external loads (i.e., compliance). 'Stiff' here means joints largely resist against external loads (Pratt, 2002). Therefore, the VAAM facilitates AMOS II interactions with different conditions.

5. Discussion

Most of the relevant discussion points had been treated in the above sections. Here, we briefly discuss only some remaining issues concerning different controllers (i.e., force/torque control) in comparison to our controller.

When confronted with perturbations (e.g., hand pushing), robots should be able to behave compliantly in order to protect themselves from damages. In addition, they should also be able to return to an original posture when the perturbation disappears (i.e., push recovery). Several works have employed different controllers to generate push recovery in their robotic systems. For example, Stephens and Atkeson (Stephens *et al.*, 2010) developed a predictive model relying on force/torque feedback on each joint of a humanoid robot where each joint is driven by a hydraulic actuator. The model allows the humanoid robot to perform push recovery, thereby stabilizing its body after perturbations are applied. Havoutis *et al.* used virtual model control for a quadruped robot (i.e., HyQ) which is a fully torque-controlled hydraulically actuated robot. His virtual model controller relies on force/torque feedback on each joint of the robot (Havoutis *et al.* 2012).

In contrast, the presented VAAM only relies on force sensing at the end effector of each leg rather than force/torque feedback on each joint. It also allows our hexapod robot to perform push recovery with variably compliant motions. Variable compliance can be simply achieved by adjusting the damping parameter of the VAAM. This achievement differs from compliance control that results from contact and vibration mechanics of braided pneumatic actuators (BPAs) (Caldwell *et al.*, 1993). However, such BPAs mechanisms make robots more bulky and mechanically complex (Kingsley *et al.*, 2006), which are difficult to be applied to small legged robots. Besides, the push recovery of the hexapod robot does not depend on hydraulic actuators instead here standard servo motors were used, one motor for each joint. We would like to also emphasize that the presented joint control mechanism based on the VAAM shows muscle-like functions.

In future work, we will apply a modular neural network (Manoonpong *et al.*, 2008) where neural outputs of the network will control muscle activations as active elements. In addition, learning mechanisms will be applied to automatically adjust VAAM's parameters for generating proper compliant locomotion with respect to different terrains. This will enable AMOS II to efficiently and naturally traverse through different terrains.

6. Acknowledgements

This research was supported by the Emmy Noether Program of the Deutsche Forschungsgemeinschaft (DFG, MA4464/3-1), the Federal Ministry of Education and Research (BMBF) by a grant to the Bernstein Center for Computational Neuroscience II Göttingen (01GQ1005A, project D1), and European Community's Seventh Framework Programme FP7/2007-2013 (Specific Programme Cooperation, Theme 3, Information and Communication Technologies) under grant agreement no. 270273, Xperience. We also would like to thank Frank Hesse, Sakyasingha Dasgupta and Tomas Kulvicius for their fruitful discussions.

REFERENCES

- Ahn A. N. (2012), "How muscles function the work loop technique", *Journal of Experimental Biology*, vol. 215, no. 7, pp. 1051-1052.
- Ahn A. N. and R. J. Full (2002), "A motor and a brake: two leg extensor muscles acting at the same joint manage energy differently in a running insect", *Journal of Experimental Biology*, vol. 205, no. 3, pp. 379-389.
- Biewener A. A. (2003), *Animal Locomotion*, Oxford Animal Biology Series, Oxford University Press.
- Caldwell, D.G., Medrano Cerda, G.A., Goodwin, M.J. (1993), "Braided pneumatic actuator control of a multi-jointed manipulator," *Systems, Man and Cybernetics*, 1993. *Systems Engineering in the Service of Humans*, *Conference Proceedings*, International Conference on , vol., no., pp.423,428 vol.1, 17-20.
- Daley M. A. and A. A. Biewener (2006), "Running over rough terrain reveals limb control for intrinsic stability", *Proceedings of the National Academy of Sciences*, vol. 103, no. 42, pp. 15681-15686.
- Dickinson M. H., C. T. Farley, R. J. Full, M. A. R. Koehl, R. Kram, and S. Lehman (2000), "How animals move: An integrative view", *Science*, vol. 288, no. 5463, pp. 100-106.
- Dudek D. M. and R. J. Full (2006), "Passive mechanical properties of legs from running insects", *Journal of Experimental Biology*, vol. 209, no. 8, pp. 1502-1515.
- Farahat WA, Herr HM (2010), "Optimal Workloop Energetics of Muscle-Actuated Systems: An Impedance Matching View", *PLoS Comput Biol* 6(6): e1000795.
- Fish F. E. (2002), "Balancing requirements for stability and maneuverability in cetaceans", *Integrative and Comparative Biology*, vol. 42, no. 1, pp. 85-93.
- Full R., D. Stokes, and A. N. Ahn (1998), "Energy absorption during running by leg muscles in a cockroach", *Journal of Experimental Biology*, vol. 201, no. 7, pp. 997-1012.
- Full R. J., T. Kubow, J. Schmitt, P. Holmes, and D. Koditschek (2002), "Quantifying dynamic stability and maneuverability in legged locomotion", *Integrative and Comparative Biology*, vol. 42, no. 1, pp. 149-157.
- Gabaldon A. M., F. E. Nelson, and T. J. Roberts (2004), "Mechanical function of two ankle extensors in wild turkeys: shifts from energy production to energy absorption during incline versus decline running", *Journal of Experimental Biology*, vol. 207, no. 13, pp. 2277-2288.
- Haeue D. F. B., S. Grimmer, and A. Seyfarth (2010), "The role of intrinsic muscle properties for stable hopping stability is achieved by the force velocity relation", *Bioinspiration & Biomimetics*, vol. 5, no. 1, p. 016004.
- Ham R., T. Sugar, B. Vanderborght, K. Hollander, and D. Lefeber (2009), "Compliant actuator designs", *Robotics Automation Magazine, IEEE*, vol. 16, pp. 81-94.
- Havoutis J. B. I., C. Semini and D. Caldwell (2012), "Progress in quadrupedal trotting with active compliance", in *Dynamic Walking 2012*, Pensacola, Florida, USA.
- Kingsley, D.A., Quinn, R.D., Ritzmann, Roy E. (2006), "A Cockroach Inspired Robot With Artificial Muscles," *Intelligent Robots and Systems, 2006 IEEE/RSJ International Conference on* , vol., no., pp.1837,1842, 9-15.
- Manoonpong P., F. Pasemann, and F. Wörgötter (2008), "Sensor-driven neural control for omnidirectional locomotion and versatile reactive behaviors of walking machines", *Robotics and Autonomous Systems*, vol. 56, no. 3, pp. 265-288.
- Nishikawa K., A. A. Biewener, P. Aerts, A. N. Ahn, H. J. Chiel, M. A. Daley, T. L. Daniel, R. J. Full, M. E. Hale, T. L. Hedrick, A. K. Lappin, T. R. Nichols, R. D. Quinn, R. A. Satterlie and B. Szymik (2007), "Neuromechanics: an integrative approach for understanding motor control", *Integrative and Comparative Biology*, vol. 47, no. 1, pp. 16-54.
- Pratt G. A. (2002), "Low impedance walking robots", *Integrative and Comparative Biology*, vol. 42, no. 1, pp. 174-181.
- Schmitt S., D. F. B. Haeue, R. Blickhan, and M. Guenther (2012), "Nature as an engineer: one simple concept of a bio-inspired functional artificial muscle", *Bioinspiration & Biomimetics*, vol. 7, no. 3, p. 036022.
- Sponberg S. and R. J. Full (2008), "Neuromechanical response of musculo-skeletal structures in cockroaches during rapid running on rough terrain", *Journal of Experimental Biology*, vol. 211, no. 3, pp. 433-446.
- Sponberg S., T. Libby, C. H. Mullens, and R. J. Full (2011), "Shifts in a single muscle's control potential of body dynamics are determined by mechanical feedback", *Philosophical Transactions of the Royal Society B: Biological Sciences*, vol. 366, no. 1570, pp. 1606-1620.
- Stephens B. and C. Atkeson (2010), "Dynamic balance force control for compliant humanoid robots", in *Intelligent Robots and Systems (IROS)*, 2010 IEEE/RSJ International Conference on, pp. 1248-1255, oct. 2010.
- Tu, M. S. and M. H. Dickinson (1996), "The control of wing kinematics by two steering muscles of the blowfly (*Calliphora vicina*)", *J. Comp. Physiol. A*, 178(6): 813-830.
- Vanderborght B., A. Albu-Schaeffer, A. Bicchi, E. Burdet, D.G. Caldwell, R. Carloni, M. Catalano, O. Eiberger, W. Friedl, G. Ganesh, M. Garabini, M. Grebenstein, G. Grioli, S. Haddadin, H. Hoppner, A. Jafari, M. Laffranchi, D. Lefeber, F. Petit, S. Stramigioli, N. T. Sagarakis, M. Van Damme, R. Van Ham, L.C. Visser, S. Wolf (2013), Variable impedance actuators: A review, *Robotics and Autonomous Systems*, Volume 61, Issue 12, Pages 1601-1614.
- Xiong X., F. Wörgötter, P. Manoonpong (2013), "A simplified variable admittance controller based on a virtual agonist-antagonist mechanism for robot joint control", in *Intl Conf. on Climbing and Walking Robots CLAWAR 2013*, Sydney, Australia, pp. 281-288.
- Zill S., J. Schmitz, and A. Bueschges (2004), "Load sensing and control of posture and locomotion", *Arthropod Structure & Development*, vol. 33, no. 3, pp. 273-286.

Corresponding author

Xiaofeng Xiong can be contacted at: Xiaofeng.Xiong@phys.uni-goettingen.de